Wideband Multi-Arm Bowtie Antenna for Millimeter Wave Electro-Optic Sensors and Receivers

Farzad Mokhtari-Koushyar*, Elham Heidari*, Hamed Dalir*, Chi-Jui Chung, Xiaochuan Xu, Volker J. Sorger, *Senior Member, IEEE & OSA*, Ray T. Chen, *Fellow, IEEE & OSA*

***Abstract*—We propose and demonstrate a novel design of a multi arm bowtie antenna (MABA) able to provide wideband field enhancement (FE). FE is a looked-for parameter of antennas in integrated electro-optic (EO) communication and sensing applications. In the proposed MABA, the paralleled arms with different lengths and flare angles provide multiple resonance frequencies. By tailoring these resonance frequencies adequately close to each other, a wide range of frequencies with high FE is achieved and the intrinsic limitation of conventional bowtie antennas in this regard is overcome. The proposed MABA is designed at the center frequency of 66.2 GHz and fabricated on a silicon on insulator (SOI) substrate with 1.69 mm × 0.21 mm dimensions. Simulation and measurement results show about 40° beam width and 63.4 dB FE peak with 27 GHz bandwidth which is 3 times larger than the bandwidth of a conventional bowtie antenna (BA), as the most commonly used antenna for this application, on the same substrate. A figure of merit (FoM) is proposed to study the performance of antennas for integrated EO applications approximately independent from the effects of substrate, operating frequency, and optical parts. The FoM is calculated and a comparison is presented for different state-of-the-art antennas in literature showing 2.28 times better performance of the proposed MABA.**

***Index Terms*— 5G networks, bowtie antenna; electro-optics; field enhancement; microwave photonics; millimeter waves; sensing; silicon; plasmonics**

I. Introduction

ANTENNA integrated electro-optic (EO) modulators and photodiodes have recently attracted interest for different applications in sensing, direct conversion of electromagnetic waves (EMW) to optical waves in receivers, and imaging [1-10]. The magnified EMW by the antenna being directly modulated on an optical carrier suggests an efficient alternative for radio frequency (FR) front-end electronics in many devices and systems such as MIMO, deinterleaving, and sensor fusion applications. As photonic EMW sensors [7], small foot print, wide bandwidth, high sensitivity, immunity to electromagnetic interference (EMI), and high speed and passive operation are their prominent advantages over their conventional electronic-based counterparts [11-13]. The modulated light can be either delivered to a photo-detector to down convert it to base band or it can be connected to optical systems and radio over fiber transceivers for communication applications [2]. The second approach provides benefiting from compact optical true time delay components [14], wide bandwidth and fast switches in optically addressed phased array antennas [8-10]. Efficiency and insertion loss of these antenna integrated EO devices can be improved even more by integrating the driving laser and/or photo detectors on the same chip [15].

The large unlicensed bandwidth, small size of antennas, and interference rejection continuously increase broad range of applications of millimeter waves (MMWs) band for 5G indoor wireless communication [16, 17], imaging systems [8, 17-19], and automotive radar sensors [20]. However, covering the potential bandwidth provided in the MMW band prohibitively increases the cost of RF front-end electronics. So, the benefits of antenna integrated EO sensors/receivers become even more demanding in MMW band. In electronic based MMW transceivers, sensors and phased array antennas, usually active electronics are the bandwidth limiting components. However, with recent advances in EO modulators [21-23], the active optical parts of photonic EO based devices can easily perform at MMW band and the integrated antennas are the bandwidth limiting components.

Although various types of components like plasmonic phased modulators [4], one-dimensional photonic crystal waveguide (PCW) [1], two-dimensional slot PCW [3], polymer and strip waveguide phase modulators [2, 5, 6], traveling wave optical waveguide [13], and photodiodes [24] are suggested in the literature for the EO part, simple and conventional antennas like dipoles [13], bowtie antennas (BA) [1, 3-5, 24,25], and slotted patch antennas (SPA) [2, 6] are employed. Regardless of the type of the active EO part, the integrated antenna directly determines the device bandwidth, radiation pattern or spatial acceptance angle. It also plays an important role in device sensitivity, efficiency, and size. In designing the antennas for

This is work is supported by the Air Force Office of Scientific Research (AFOSR) Small Business Innovation Research (SBIR) program award number FA9550-17-P-0014 under the guidance of Dr. Gernot Pomrenke.

F. Mokhtari-Koushyar, E. Heidari, C.J. Chung, and R. T. Chen are with the Microelectronic Research Center, Department of Electrical and Computer Engineering, University of Texas, Austin, TX 78758, USA (emails: mokhtari@utexas.edu; e.heidari@utexas.edu; cjchung@utexas.edu; chen@ece.utexas.edu).

H. Dalir and X. Xu are with Omega Optics, Inc., Austin, TX 78757, USA (e-mails: hamed.dalir@omegaoptics.com and xiaochuan.xu@omegaoptics.com).

V. J. Sorger is with Department of Electrical and Computer Engineering, The George Washington University, Washington, DC 20052, USA (e-mail: sorger@gwu.edu).

*The authors contributed to the paper equally.

This article has been accepted for publication in a future issue of this journal, but has not been fully edited. Content may change prior to final publication. Citation information: DOI 10.1109/JLT.2018.2842712, Journal of Lightwave Technology

integrated EO applications field enhancement (FE) is the most important parameter and bandwidth of the antenna is determined by the bandwidth of FE. The larger the FE, the higher sensitivity in sensing applications, the larger signal to noise ratio in communications, and the larger dynamic range in imaging systems. A wide bandwidth of FE also provides higher capacity in communications and larger information collected in sensing and imaging applications.

Patch antennas are not usually considered as wideband antennas [26]. Accordingly, SPAs such as the antenna proposed in [2] with about 60 dB FE and 5 GHz bandwidth at 60 GHz or the one proposed in [6] with 36 dB FE and 2 GHz bandwidth at 36 GHz provide less than 10% fractional bandwidth. Among the suggested antennas for integrated EO devices, BAs offer between 20-30% fractional FE bandwidth. For example, the BA with very narrow flare angle in [4] presents about 87 dB FE with 14 GHz bandwidth at 60 GHz. The BAs with 60˚ flare angle reported in [1] and [3] along with highly doped silicon regions demonstrate a slot with about 64.3 dB FE with 4.84 GHz bandwidth at 14.1 GHz and about 78 dB FE with 5 GHz bandwidth at 10 GHz, respectively. A large 90˚ flare angle BA in [5] has about 33 dB FE with 5 GHz bandwidth at 15 GHz. But even BAs have a limit in providing high FE and wideband FE at the same time.

In this paper, we first discuss the methodology of designing an antenna for integrated EO applications. As we will discuss, in contrast to conventional antennas, EO antennas should not be designed with 50 Ohm input impedance, but with impedances as high as possible. Then, the limit of BAs in simultaneously providing large and wideband FE is addressed. This limit originates from the incapability of BAs in delivering large and wideband impedance at the same time. Next, a novel multi-arm bowtie antenna (MABA) is proposed to overcome this limit. The design features multiple arms with small flare angles that yield to adjacent impedance large peaks (or equivalently resonance frequencies). Each of these resonance frequencies leads to a large FE over a relatively narrow frequency band. Tailoring these impedance peaks adequately close to each other, a wide range of large FE is achieved. The proposed structure is fabricated on a silicon on isolator (SOI) wafer. Upon interrogating the antenna, we observe 63.4 dB FE with 27 GHz FE at 66.2 GHz via simulation and measurement results. The achieved response is three times wider than the FE bandwidth a conventional BA can provide on same substrate. Next, a figure of merit (FoM) is proposed to study the antenna performance approximately independent of the EO part, substrate effect, and center frequency. Finally, the FoM is calculated for different antennas proposed in the literature for this application and the results are summarized.

II. Antenna Integrated EO Sensors and Receivers

EO sensors and receivers usually rely on Pockels or Kerr effects that create variations in the refractive index of an optical waveguide, Δn, by applying an electrical field, E, provided by the integrated antenna [1-10] at an EO material. In Pockels effect Δn is proportional to electrical field as stated in (1),

$$\Delta n = \frac{1}{2} n_{eff}^3 \, \Gamma E \tag{1}$$

where Γ is the overlap integral factor defined as the convolution of the optical guided mode with the applied electric field in the EO material and n_{eff} is the effective refractive index of the optical mode in the waveguide. Similar formulation can be written for Kerr effect where Δn is proportional to square of the electrical field. To enhance the sensitivity of EO sensors and receivers, the ΓE product should be enhanced as much as possible. As shown in the inset of Fig. 1 (a), by proper designing of the antenna Γ can be increased close to its maximum value where the electrical and optical fields are confined in the slot. E is determined by antenna performance and is evaluated by a FE factor defined as the ratio of the amplitude of electrical field at the center of optical waveguide with and without presence of the antenna. FE can be expressed as [4],

$$FE = \frac{|E|}{|E_0|} = \frac{\lambda\sqrt{GZ}}{W_s\sqrt{4\pi Z_0}} \tag{2}$$

where W_s is width of the slot between the antenna arms (see Fig. 1), E_0 is incident electrical field, Z_0 is chracteristic impedance of free space, Z is antenna impedance, G is realized gain of the antenna which includes dielectric loss of the substrate and ohmic loss due to gold imperfections, and λ is wavelength of electrical field. Therefore, Δn can be expressed as follows.

$$\Delta n = \frac{1}{2} n_{eff}^3 \Gamma E_0 \times FE \tag{3}$$

It's noteworthy that polarization of E_0 is assumed to be matched with polarization of the antenna. And polarization of E needs to be matched with the direction in which the EO material provides EO effect. This direction is determined by the crystal axis in EO materials like lithium niobite ($LiNbO_3$) [2, 13] and by poling direction in EO polymers [1, 3-6, 22]. This polarization matching can be achieved by properly designing the antenna electrodes as shown in the inset of Fig. 1 (a). These electrodes distribute the received electrical field uniformly over the optical waveguide and EO material. Any polarization mismatch needs to be considered in (1) and (2).

From (2) and (3) it can be said that in contrast to antennas for conventional applications where 50 or 75 Ohm impedance is desired, for integrated EO applications antenna impedance should be designed as high as possible. This means the power received by the antenna should be converted to a large electric field and small magnetic field because it is the electrical field that perturbs the EO material whereas the magnetic field plays no role. Additionally, bandwidth of the antenna is determined by bandwidth of FE, not bandwidth of reflection loss.

III. Multi-Arm Bow-Tie Antenna

In this section, first, the trade-off of a conventional BA, which is most commonly used antenna for EO integrated application, between large FE and wideband FE is discussed

This article has been accepted for publication in a future issue of this journal, but has not been fully edited. Content may change prior to final publication. Citation information: DOI 10.1109/JLT.2018.2842712, Journal of Lightwave Technology

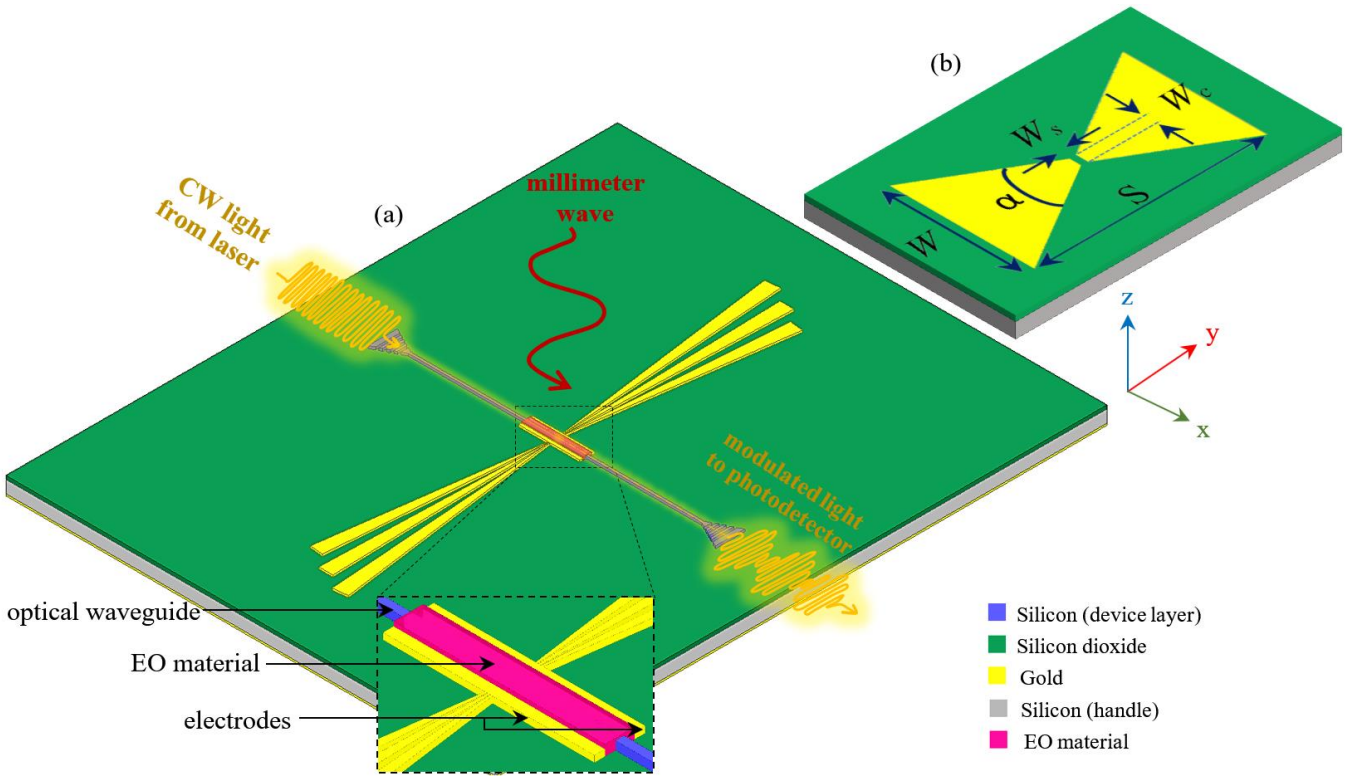

Fig. 1. (a) The multi-arm bowtie antenna design integrated in electro-optic sensor/reciever, and (b) convetional bowtie antenna both on silicon-on-insulator wafer.

and then overcoming of the proposed MABA to this limit is demonstrated.

A. *Limitations of Conventional Bowtie Antenna*

To achieve a large FE based on (2), minimum possible value of W_s is desired while W_s is usually limited by either the width of optical waveguide or by fabrication errors. For plasmonic waveguides W_s can be as low as tens of nanometers [4, 22,25] while for conventional and PCWs it is about a few microns [1, 3, 27]. W_c is usually determined by the required length of the optical waveguide (interaction length) in the antenna slot. For lossy plasmonic waveguides, interaction length is limited to tens of micrometer while for PCWs with relatively lower loss, interaction length can be increased up to hundreds of microns. As depicted in Fig. 1 (b), the remaining design parameters of a conventional BA are α, and S which are flare angle and arm length, respectively. In fact, α determines the impedance of the antenna and S scales the resonance frequency [26, 28].

Fig. 2 (a) shows simulation results of the inherent limit of a BA in providing large and wideband FE at the same time. This limit originally comes from the behavior of impedance of the antenna which is depicted in Fig. 2 (b) and (c). Table I lists the parameters used in the simulations where W_s is selected to be matched with the modulator presented in [28], however, 1 µm can be considered as a typical number to assess the antenna performance independent from the optical modulator. To extract the effect of the arm length, S, which is simply a frequency scaling (as far as material properties are constant [26]), the frequency axis is normalized to the resonance frequency of first dominant mode, TM_{01}, of the case where α=30˚. To increase the antenna efficiency, which is reflected in realized gain, G, in (2), the antenna should be designed close to its resonance frequency. As can be seen from Fig. 2 (b) and (c), there are two regions of impedance: First is the slowly varying region around $f/f_r \approx 0.5$ where the reactance is crossing close to zero and the antenna

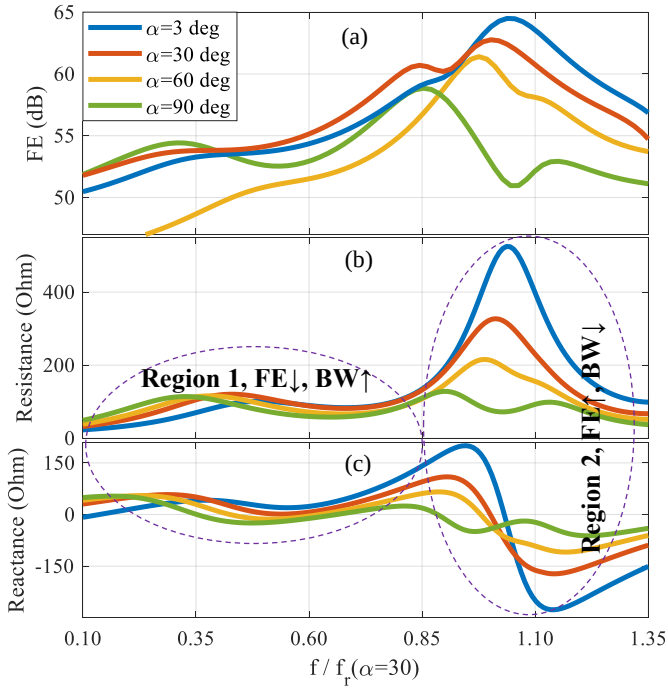

Fig. 2. Simulation resutls of (a) field enhancement (FE), (b) real part of impedance or resistance, and (c) imagenary part of impedance or reactance of a conventional bowtie antenna depicted in Fig. 1(b) versus normalized frequcecy (to the resonance frequcny of the dominant TM_{01} mode of the BA with α=30˚). Other parameters of the simulations are given in Table I.

This article has been accepted for publication in a future issue of this journal, but has not been fully edited. Content may change prior to final publication. Citation information: DOI 10.1109/JLT.2018.2842712, Journal of Lightwave Technology

resistance varies smoothly. This region leads to a relatively wideband FE with small values of FE (about 12 dB less than the peak of FE in the second region). The second region is the frequency range around $f/f_r \approx 1$ where the fast resonance creates large values of resistance and consequently large FE peaks. But the FE bandwidth in the second region is about one third of the first region. A BA can be designed and used in either of these regions, but it cannot provide large and broadband FE at the same time as discussed.

TABLE I. DESIGN AND SIMULATIONS PARAMTERES

PARAMETER	VALUE
Gold thickness	400 nm
Silicon device layer thicknes	220 nm
Silicon dioxide thickness	3 µm
Silicon handle layer thickness	625 µm
Interaction length, W_c	50 µm
Slot width, W_s	1 µm
Silicon permitivity	11.9
Silicon dioxide permitivity	4
Silicon bulk resistivity	125 Ohm-cm

B. *Multi-Arm Bowtie Antenna*

The structure of the proposed MABA is depicted in Fig. 1 (a) where multiple bowties with different flare angles and arm lengths are shunted. Each of these arms provides a large FE around its resonant frequency (i.e. the second region in Fig. 2) with a limit bandwidth. So, by properly designing the resonances of these arms adequately close to each other, a wide range of the frequency can cover a large range of FE values. Although shunting multiple arms reduces the equivalent impedace of the antenna, selecting very small flare angles for the arms compensates this reduction by providing a rather large impedance for each arm. The added electrodes, shown in the inset of Fig.1 (a), distribute the captured field uniformly over the interaction length with optical waveguide and EO material. These electrodes act as a capacitor shunted with the antenna and shifts their resonance frequencies. Due to this frequency shift and the strong coupling between arms, their resonance frequencies must be obtained via numerical simulations, as undergone here.

C. *Design and Simulations*

Here we present an optimized widenband design of the proposed antenna for MMW EO sensing/receiving application. To this end, three different arms lengths, namely S_1=1.694 mm, S_2=1.456 mm, S_3=1.280 mm, and α=3.5º for all of arms and 2º axis-to-axis spacing between them, are used. Although a larger number of arms might provide a even wider bandwidth, there is a trade-off between the impedance of the antenna and FE bandwidth. Therefore, to obtain larger FE we cover the required frequcny range with minimum possible number of arms. Since here we propose the antenna independent from EO part, the electrodes are consired to be 2.5 µm wide and 50 µm long with a 1 µm gap in between them as typical values. The effect of these electrodes is discussed more deeply in the next section. Other paramteres are the same with conventional BA as listed in Table. I. The full-wave three-dimensional (3D) simulations are done by Ansys Electronics Desktop [30]. As presented in the simulation results in the next section along with measurement results, these three arms create three adjacent impedance peaks at 57, 69, and 78 GHz that altogether provide 26.97 GHz range of relatively flat FE from 52.72 to 79.69 GHz with an average FE of 60.46 dB. The normalized FE over the antenna depicted in Fig. 3 (a) clearly shows how the field received by the antenna is focused uniformly between the electrodes. Also, vector field depicted at the cross section of the electrodes in Fig. 3 (b) shows the direction of the enhanced field which should be parallel with the direction of EO effect in the EO material.

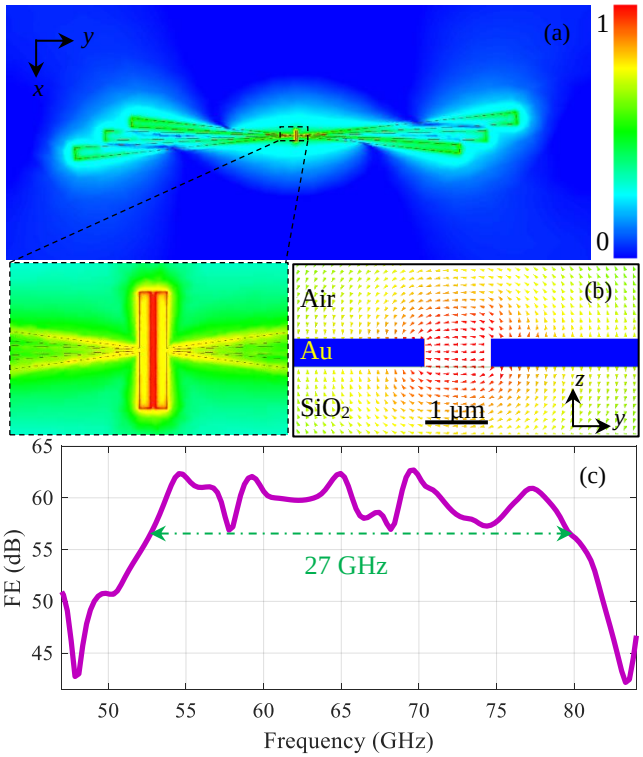

Fig. 3. (a) Top view (x-y plane) of normalized field enhancement (FE) over the multi-arm bowtie antenna and (b) cross section view (y-z plane) of normalized electrical field over the antenna slot both in logaritmic scale (c) field enhancement of the proposed antenna depicted in Fig. 1(a).

IV. FABRICATION AND MEASUREMENTS

As explained before, a key parameter of an antenna for integrated EO applications is FE. However, due to small size of the antenna slot, FE cannot be measured directly. Moreover, the small wavelength of MMWs compared to the size of field probes, makes it more difficult to measure the electromagnetic field without disturbing it. The FE between the two opposing metallic arms can be calculated indirectly from modulation index measurement results [1, 4] based on (1). To evaluate the antenna performance independent directly from RF

This article has been accepted for publication in a future issue of this journal, but has not been fully edited. Content may change prior to final publication. Citation information: DOI 10.1109/JLT.2018.2842712, Journal of Lightwave Technology

measurements, here we added a tapered differential microstrip line (DML) to feed the antenna using a 50 Ohm 100 µm pitch ground-signal (GS) probe. As depicted in Fig. 4 (a) the DML including two traces with 140 µm width and an 8 µm gap in between them is designed to have 50 Ohm impedance for its odd mode to be matched with the GS probe. Then, the DML is tapered down to two electrodes with a 1 µm gap in between as depicted in Fig. 4 (b). The length of the feed line (L_{feed}), length of the tapering (L_{taper}), and electrodes length are 1.55 mm, 1.45 mm, and 50 µm, respectively. In this way, the impedance and realized gain of the antenna can be measured from the end of DML. In the next section, fabrication process of the device is explained.

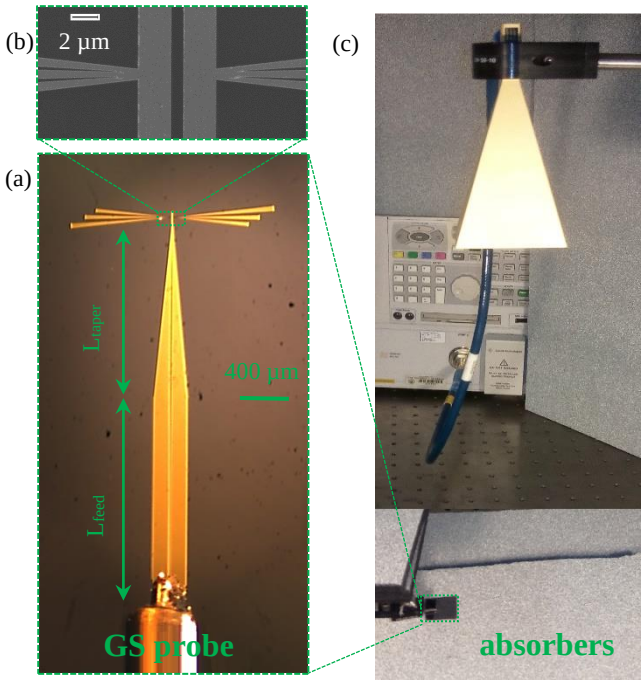

Fig. 4. (a) CCD camera image of the fabricated multi-arm bowtie antenna feeded with a tapered 50 Ohm differential microstrip line, (b) SEM image of the slot and electrodes of the proposed antenna, and (c) measurement setup consisting of horn antenna connected to a network analyzer and multi-arm bowtie antenna connected to the other part via depicted ground-signal probe.

A. Fabrication Method

The antenna is fabricated on a SOI platform. All the components including transmission lines and antennas are patterned using the JEOL JBX-6000FS electron-beam lithography tool with ZEP-520A e-beam resist, followed by developing in n- Amyl acetate for 2 minutes, and rinsing in isopropyl alcohol. The waveguide and antenna were defined using a metal hard mask, which was patterned using electron beam lithography. A 400 nm Au was deposited via E-beam evaporator and lift-off process were followed with Remover PG. The sample were then cleaned and cleaved so that the antenna was placed at the center of the chip. Fig. 6 (a) shows the image of the antenna under measurements taken by a charge-coupled device (CCD) camera with 50X zoom. The scanning electron microscopy (SEM) image of the antenna slot and electrodes taken by Carl SEM ZEISS Neon 40.

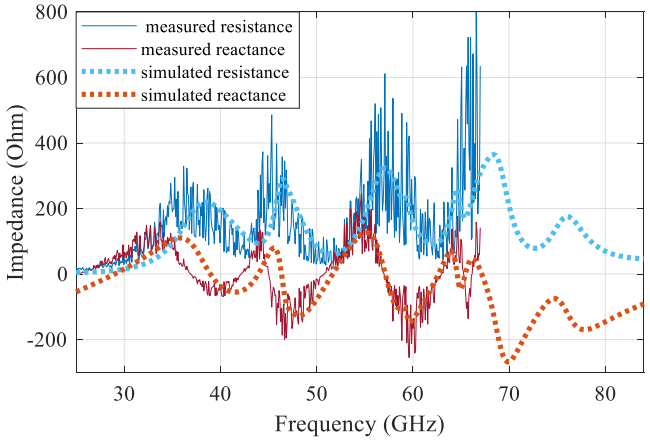

Fig. 5. Simulation (dashed lines) and measurement ressutls of (a) real (blue lines) and imagenary (red lines) part of impedance showing three impedance peaks at at 57, 69, and 78 GHz.

B. Measurement Setup

As depicted in Fig. 4 (c), the measurement setup includes a standard gain horn antenna with 20 dBi gain and 11º beam width in both azimuth and elevation directions to illuminate the MABA from 30 cm center-to-center distance. Using the CCD camera and 3D microprobe stages, the GS microprobe is placed on antenna feed line. After mounting the GS probe, the CCD camera is moved from measurement area. The horn antenna and the proposed antenna are then connected to an Agilent E8361 67 GHz network analyzer. Therefore, the frequency range of our measurement is limited from 25 GHz, which imposed by the horn antenna, to 67 GHz, the highest frequency of the network analyzer. However, our frequency range of interest is 60 to 90 GHz. Five layers of absorber sheets with more than 45 dB isolation are deployed under the sample chip to prevent reflections from the metallic parts of the optical table. Metallic parts of the probe stations are covered with absorber sheets too, as shown in Fig. 4 (c). Effects of the cables and connectors are excluded by short-load-open-throu calibration method.

C. Results and Discussions

S_{11} measurements with MABA being connected to the first channel of the network analyzer are exploited to calculate the antenna impedance. To this end, transmission line equation is used to transfer the impedance seen from the end of DML to the impedance seen from electrodes [31]. Measurement results of 50 iterations are averaged to boost signal to noise ratio. But, due to multiple division operations in calculating impedance, the small noise in measured S_{11} is amplified again. Despite this, a good agreement between measurement and simulation results in Fig. 5 can be seen. In the frequency range of interest (60 to 90 GHz) three adjacent impedance peaks are observed at 57.16, 68.40, and 76.23 GHz. Value of the impedance is determined by the flare angles of the arms and the conductivity of substrate.

Also, S_{12} measurements are employed to calculate the antenna realized gain in different frequencies from Friis' transmission equations [26]. Since MABA is not designed for 50 Ohm impedance, a large reflection loss between the antenna and its feed is expected. So, it is important to include the

This article has been accepted for publication in a future issue of this journal, but has not been fully edited. Content may change prior to final publication. Citation information: DOI 10.1109/JLT.2018.2842712, Journal of Lightwave Technology

reflection loss terms in Friis' equation as follows.

$$\frac{P_r}{P_t} = G_t G_r (\frac{\lambda}{4\pi R})^2 (1-|\Gamma_t|^2)(1-|\Gamma_r|^2) \quad (4)$$

where P_t and P_r are the transmitted and received power, respectively. So, the ratio of P_r/P_t is equal to $|S_{12}|^2$ in our measurement setup. Γ_t and Γ_r are the reflection coefficients of the horn antennas and the MABA antenna. The reflection coefficients can be calculated from S_{11} and S_{22} measurements. In fact, the GS probe and DML are matched and the major reflection happens between the feed line and electrodes. Using the calculation of impedance in previous section, Γ_r can be expresses as:

$$\Gamma_r = \frac{Z - Z_{DML}}{Z + Z_{DML}} \quad (5)$$

where Z_{DML} is characteristic impedance of feed and tapering section at each frequency. Fig. 6 shows the calculated realized gain based on the measured S parameters. The calculated gain includes the dielectric loss and metallic loss, however, the port mismatches are excluded bashed on (4). In the frequency range of interest, three peaks of gain are observed at 53.46, 63.01, and 75.72 GHz. These peaks happen at frequencies slightly different from impedance peaks in a way that their product yields to a relatively flat FE based on (2).

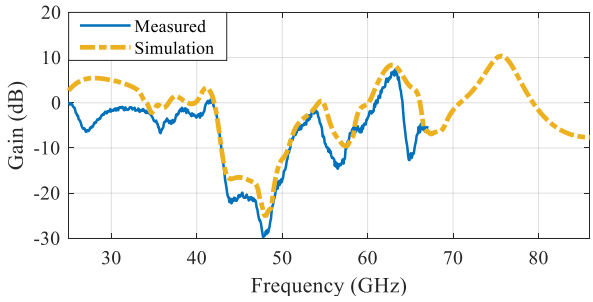

Fig. 6. Simulation (dashed yellow line) and measured (solid blue line) resutls of gain of the fabricated multi-arm bowtie antenna depicted in Fig. 3 (a) at φ=0˚ and θ=0˚ direction.

The calculated FE based on the gain and impedance measurements from (2) is demonstrated in Fig. 7. We find a decent agreement between the simulation and measurement results, thus not only confirming MABA performance but also proving the validity of the method used to indirectly measure the FE. Since, the results in the measured frequency range follows the simulation results, the same trend can be expected in higher frequencies as well. From 52.27 GHz to 67 GHz, the overlap of our target frequency range and the span the measurement setup covers, an average value of 2.43 dB decrement is observed in the FE. This reduction can be assigned to the thickness of deposited gold compared to the gold skin depth in MMW ranges. At the center frequency of the span shown in Fig. 3 (c), 66.20 GHz, gold skin depth is 293 nm. So, thickness of the deposited gold (limited by our fabrication facility) is 1.37 of the skin depth which can be translated to more metal loss than what is normally considered. The larger decrement of FE at lower frequencies, where the skin depth becomes deeper, endorses the metallic loss being the reason of this depression. For example, at 35 GHz there is 5.12 dB difference between simulation and measurement results where the skin depth is 402 nm. This problem is solvable by deposing thicker layer of the gold. Actually, 3 to 5 times of skin depth at the desired frequency is required to consider the gold a near perfect conductor.

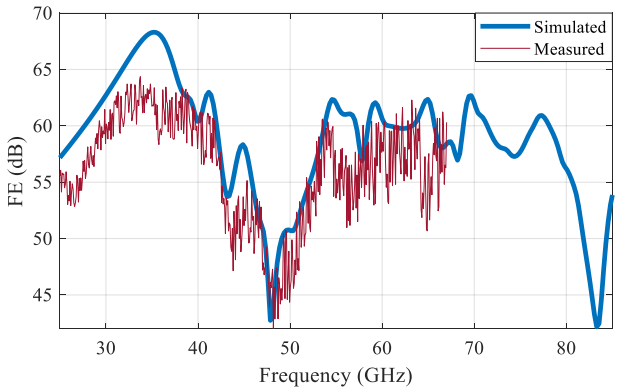

Fig. 7. Calculated field enhancement (thin red line) based on (2) from the gain and impedance measurements and simulated field enhacement (thick blue line).

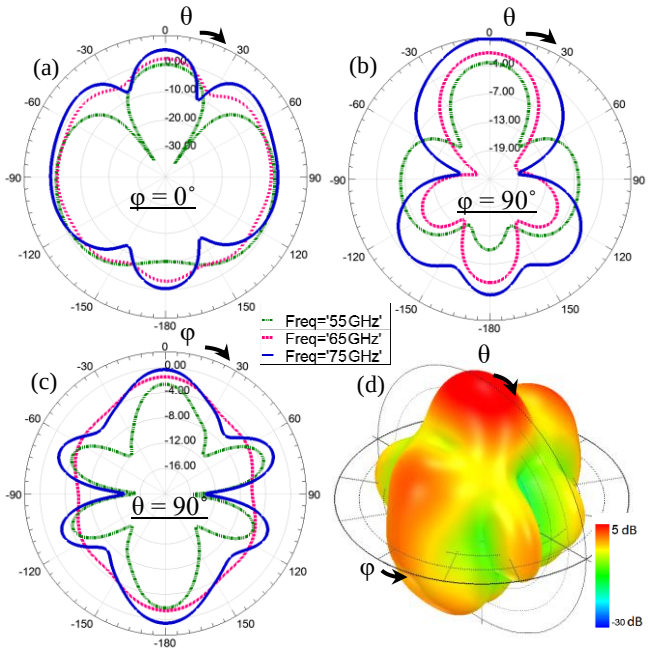

Fig. 8. Simulated gain pattern of the proposed antenna at 55 GHz (dsahed green line), 65 GHz (doted red line) and 75 GHz (solid blue line); (a) in elevation direction when φ=0˚, (b) in elevation direction when φ=90˚, and (c) in azimuth direction when θ=90˚. (d) Three dimentional gain pattern at 65 GHz.

So, compared to the convetional BA with α=3˚, by sacrificing 1.73 dB of FE peak the bandwidth is increased by 3 times. It worth mentionening that either in electro-absortive or interferometer-based electro-refrative EO sensors and recievers, the output optical power is propotional to the square of the FE. Therefore, 3 dB half-power bandwith of the output optical power is corresponding to 6 dB bandwidth of the FE. The two outer arms of the proposed MABA have 5.5º misalignment with incoming y-polarized MMW which creates

This article has been accepted for publication in a future issue of this journal, but has not been fully edited. Content may change prior to final publication. Citation information: DOI 10.1109/JLT.2018.2842712, Journal of Lightwave Technology

less than 1% polarization mismatch loss. Radiation pattern of the proposed antenna is presented in Fig. 8 in different planes. As can be seen, the antenna preserves its main lobe in $\theta=0^\circ$ and $\varphi=0^\circ$ direction when frequency changes from 55 GHz to 75 GHz. The main lobe provides about 47˚, 40˚, 38˚ beam width and 3.96 dB, 3.68 dB, 6.48 dB side lobe level at 75 GHz, 65 GHz, and 55 GHz, respectively.

Despite of the discussed depression which is not the intrinsic limit of the proposed MABA, the proposed antenna overcomes the limitation of conventional BAs as demonstrated by simulation and measurement results. The FE bandwidth provided by proposed MABA is about three times larger than the bandwidth a similar BA can provide on the same substrate.

D. Figure of Merit

Either the antenna proposed here or others presented in the literature can be implemented on different substrates and with different EO materials and components. As expressed in section II as well as demonstrated in [2, 4] FE provided by an antenna can be increased by reducing W_s. The similar effect of W_s variation on FE in different types of antennas can be seen in Fig. 4 (b) of [2] and Fig. 3 and Fig. 5 (b) of [4]. Since W_s is not an antenna parameter and it is imposed by EO components, to provide a fair and independent comparison of FE among different antennas, we suggest to normalized FE to W_s. Additionally, since antennas are scalable components and their bandwidth is proportional to operation frequency, fractional bandwidth can be a more insightful representation of antenna bandwidth [26].

TABLE II. COMPARISON AMONG THE ANTENNAS PROPOSED FOR ELECTRO-OPTIC INTEGRATED DEVICES IN LITERATURE

Antenna type	BW (GHz)	Peak FE (dB)	f_c (GHz)	Size (mm^2)	Gap (μm)	FoM (nm)
BA [1]	4.84	~63.5	14.1	4.6×4.8	0.16	0.018
SPA [2]	~5*	~60	60	0.8×0.8	3	0.313
BA [3]	~5	~78	10	6.0×3.5	0.32	0.212
BA [4]	~14	~84	60	1.43×0.05	0.075	0.194
BA [5]	5	~33	15	10×10	10	0.015
SPA [6]	2	54	36	5.36×1.5	10	0.052
dipole [13]	8.4	-	12	~2×3	~10	-
proposed MABA	27	63.4	66.2	1.69×0.21	1	0.713

*Since the direct information isn't reported in the paper, the bandwidth of this antenna is calculated based on the device efficiency plot in [2].

Antenna size is another important factor as it is proportional to antenna effective area and therefore its gain. Antenna size which is usually the largest component in integrated EO devices defines the package density of the device too. Finally, the substrate conductivity that results in dielectric loss introduce a trade-off between antenna bandwidth and FE. Substrate loss and metallic loss either due to the metal roughness or insufficient thickness lead to a low qualify factor for the antenna as a resonator and therefore, the antenna provides wider bandwidth. However, most of the power received by the antenna is dissipated in the lossy substrates causing reduction in antenna realized gain and consequently FE. Hence, we propose product of normalized FE and fractional bandwidth divided by the largest dimension of the antenna as a FoM to study the antenna performance approximately independent from all mentioned effects as:

$$FoM = \frac{FE \times W_s \times BW}{D\, f_c} \tag{6}$$

where BW is bandwidth, D is the largest dimension of the antenna and f_c is center frequency. Table II presents a comparison of different parameters as well as dimension less FoM of the state-of-the-art antennas proposed in literature and the presented MABA in this work.

The FoM values also show at least 2.28 times better performance compared to the other conventional BAs and SPAs listed in Table II. The numbers of evaluated FoM for different antennas show the proposed FoM can appropriately quantize the performance of the antennas for integrated EO applications.

V. CONCLUSION

The proposed multi-arm bowtie antenna benefiting from large effective area and adjacent resonance frequencies of different arms and large impedance of narrow arms at the same time surpasses the limit of conventional bowtie antennas which are commonly used for EO devices. The 63.4 dB FE with a 27 GHz bandwidth demonstrated here along with recently reported high speed modulators enable EO devices for a variety range of MMW applications from 5G communications to collision avoidance radars and MMW imaging systems. The MABA structure can be easily designed for multi-band applications as well by separating the resonance frequencies more than what is presented in this wok. Also, using wider arms or substrates with lower resistivity, the presented structure can be designed for common application where a 50 Ohm impedance is required. The proposed FoM measures performance of antennas independent of EO components, operations frequency, and substrates and shows a superior performance by 2.28x as compared to state-of-the-art BAs and SPAs antenna designs.

REFERENCES

[1] C.-J. Chung, X. Xu, Z. Pan, F. Mokhtari-Koushyar, R. Wang, H. Yan, *et al.*, "Silicon-based Hybrid Integrated Photonic Chip for Ku band Electromagnetic Wave Sensing," *Journal of Lightwave Technology*, 2017.

[2] Y. N. Wijayanto, H. Murata, and Y. Okamura, "Electrooptic Millimeter-Wave–Lightwave Signal Converters Suspended to Gap-Embedded Patch Antennas on Low-k Dielectric Materials," *IEEE Journal of Selected Topics in Quantum Electronics*, vol. 19, pp. 33-41, 2013.

[3] X. Zhang, A. Hosseini, H. Subbaraman, S. Wang, Q. Zhan, J. Luo, *et al.*, "Integrated photonic electromagnetic field sensor based on broadband bowtie antenna coupled silicon organic hybrid modulator," *Journal of Lightwave Technology*, vol. 32, pp. 3774-3784, 2014.

[4] Y. Salamin, W. Heni, C. Haffner, Y. Fedoryshyn, C. Hoessbacher, R. Bonjour, *et al.*, "Direct Conversion of Free Space Millimeter

Waves to Optical Domain by Plasmonic Modulator Antenna," *Nano Letters*, vol. 15, pp. 8342-8346, 2015/12/09 2015.

[5] O. D. Herrera, K. J. Kim, R. Voorakaranam, R. Himmelhuber, S. Wang, V. Demir, *et al.*, "Silica/Electro-Optic Polymer Optical Modulator With Integrated Antenna for Microwave Receiving," *Journal of Lightwave Technology*, vol. 32, pp. 3861-3867, 2014.

[6] D. Park, V. Pagán, T. Murphy, J. Luo, A.-Y. Jen, and W. Herman, "Free space millimeter wave-coupled electro-optic high speed nonlinear polymer phase modulator with in-plane slotted patch antennas," *Optics express*, vol. 23, pp. 9464-9476, 2015.

[7] C. A. Schuetz and D. W. Prather, "Optical upconversion techniques for high-sensitivity millimetre-wave detection," in *Passive Millimetre-Wave and Terahertz Imaging and Technology*, 2004, pp. 166-175.

[8] S. Shi, J. Bai, G. J. Schneider, Y. Zhang, R. Nelson, J. Wilson, *et al.*, "Conformal wideband optically addressed transmitting phased array with photonic receiver," *Journal of Lightwave Technology*, vol. 32, pp. 3468-3477, 2014.

[9] D. D. Ross, M. R. Konkol, S. Shi, C. E. Harrity, A. A. Wright, C. A. Schuetz, *et al.*, "Low-Profile High-Power Optically Addressed Phased Array Antenna," *Journal of Lightwave Technology*, vol. 35, pp. 3894-3900, 2017.

[10] S. Shi, J. Bai, R. Nelson, C. Schuetz, P. Yao, G. J. Schneider, *et al.*, "Ultrawideband optically fed tightly coupled phased array," *Journal of Lightwave Technology*, vol. 33, pp. 4781-4790, 2015.

[11] H. Liu, J. Yu, P. Huggard, and B. Alderman, "A multichannel THz detector using integrated bow-tie antennas," *International Journal of Antennas and Propagation*, vol. 2013, 2013.

[12] G. Gustafsson, R. Boström, B. Holback, G. Holmgren, A. Lundgren, K. Stasiewicz, *et al.*, "The electric field and wave experiment for the Cluster mission," *Space Science Reviews*, vol. 79, pp. 137-156, 1997.

[13] W. B. Bridges, F. T. Sheehy, and J. H. Schaffner, "Wave-coupled LiNbO/sub 3/ electrooptic modulator for microwave and millimeter-wave modulation," *IEEE Photonics Technology Letters*, vol. 3, pp. 133-135, 1991.

[14] C.-J. Chung, X. Xu, G. Wang, Z. Pan, and R. T. Chen, "On-chip optical true time delay lines featuring one-dimensional fishbone photonic crystal waveguide," *Applied Physics Letters*, vol. 112, p. 071104, 2018.

[15] H. Dalir, M. Ahmed, A. Bakry, and F. Koyama, "Compact electro-absorption modulator integrated with vertical-cavity surface-emitting laser for highly efficient millimeter-wave modulation," *Applied Physics Letters*, vol. 105, p. 081113, 2014.

[16] L. Verma, M. Fakharzadeh, and S. Choi, "Backhaul need for speed: 60 GHz is the solution," *IEEE Wireless Communications*, vol. 22, pp. 114-121, 2015.

[17] F. Mokhtari-Koushyar and A. A. Shishegar, "Scattering analysis of human body modeled by NURBS surfaces in MM-wave band," in *Millimeter-Wave and Terahertz Technologies (MMWATT), 2014 Third Conference on*, 2014, pp. 1-4.

[18] A. Farsaei, F. Mokhtari-Koushyar, S. Javad Seyed-Talebi, Z. Kavehvash, and M. Shabany, "Improved Two-Dimensional Millimeter-Wave Imaging for Concealed Weapon Detection Through Partial Fourier Sampling," *Journal of Infrared, Millimeter, and Terahertz Waves*, pp. 1-14, 2015/11/18 2015.

[19] J. P. Samluk, C. A. Schuetz, T. Dillon, E. L. Stein, A. Robbins, D. G. Mackrides, *et al.*, "Q-band millimeter wave imaging in the far-field enabled by optical upconversion methodology," *Journal of Infrared, Millimeter, and Terahertz Waves*, vol. 33, pp. 54-66, 2012.

[20] J. Hasch, E. Topak, R. Schnabel, T. Zwick, R. Weigel, and C. Waldschmidt, "Millimeter-Wave Technology for Automotive Radar Sensors in the 77 GHz Frequency Band," *Microwave Theory and Techniques, IEEE Transactions on*, vol. 60, pp. 845-860, 2012.

[21] C. Hössbacher, A. Josten, B. Bäuerle, Y. Fedoryshyn, H. Hettrich, Y. Salamin, *et al.*, "Plasmonic modulator with> 170 GHz bandwidth demonstrated at 100 GBd NRZ," *Optics Express*, vol. 25, pp. 1762-1768, 2017.

[22] C. Haffner, W. Heni, Y. Fedoryshyn, A. Josten, B. Baeuerle, C. Hoessbacher, *et al.*, "Plasmonic organic hybrid modulators—scaling highest speed photonics to the microscale," *Proceedings of the IEEE*, vol. 104, pp. 2362-2379, 2016.

[23] H. Dalir, F. Mokhtari-Koushyar, I. Zand, E. Heidari, X. Xu, Z. Pan, *et al.*, "Atto-Joule, high-speed, low-loss plasmonic modulator based on adiabatic coupled waveguides," in *Nanophotonics* vol. 0, ed, 2018.

[24] M. R. Konkol, D. D. Ross, S. Shi, C. E. Harrity, A. A. Wright, C. A. Schuetz, *et al.*, "High-power photodiode-integrated-connected array antenna," *Journal of Lightwave Technology*, vol. 35, pp. 2010-2016, 2017.

[25] M. Chen, F. Ho, M.-C. Lin, and D. Tsai, "Localization of optical fields using a bow-tie nanoantenna," Scanning, vol. 26, pp. I113-7, 2004.

[26] C. A. Balanis, *Antenna theory: analysis and design*: John Wiley & Sons, 2016.

[27] X. Zhang, C.-J. Chung, S. Wang, H. Subbaraman, Z. Pan, Q. Zhan, *et al.*, "Integrated broadband bowtie antenna on transparent silica substrate," *IEEE Antennas and Wireless Propagation Letters*, vol. 15, pp. 1377-1381, 2016.

[28] J. George, M. Deepukumar, C. Aanandan, P. Mohanan, and K. Nair, "New compact microstrip antenna," *Electronics Letters*, vol. 32, pp. 508-509, 1996.

[29] Dalir, H., Mokhtari-Koushyar, F., Zand, I., et al. (2018). Atto-Joule, high-speed, low-loss plasmonic modulator based on adiabatic coupled waveguides. Nanophotonics, 0(0), pp. -. Retrieved 11 May. 2018.

[30] Available: http://www.ansys.com/Eletronics

[31] D. M. Pozar, "Microwave Engineering 3e," *Tramsmission Lines and Waveguides*, pp. 143-149, 2005.

Farzad Mokhtari-Koushyar obtained his M.Sc. degree from the Department of Electrical Engineering, Sharif University of Technology, Tehran, Iran. He is now pursing his PhD degree in Department of Electrical and Computer Engineering at the University of Texas at Austin, Austin, TX, USA. His research interests include RF sensing, 5G networks, phased array antennas, RF and microwave photonic devices, VCSELs, printed electronics, and photonic integrated circuits.

Elham Heidari obtained her M.Eng. from the Department of Electronic and Applied Physics, Tokyo Institute of Technology, Tokyo, Japan. She is now pursing the PhD degree in Department of Electrical and Computer Engineering, University of Texas at Austin, Austin, TX, USA. Her research interests include nano-photonics, high speed modulators, and photonic RF sensors.

Hamed Dalir received his M.S. and Ph.D. degrees in electrical engineering from the Tokyo Institute of Technology, Tokyo, Japan, in 2011 and 2014, respectively. Prior joining to Omega Optics, Dr. Dalir was a postdoctoral researcher at the Japan Society for the Promotion of Science (JSPS) and postdoctoral research associate at the University of California Berkeley in 2015 and 2016, respectively. His current research interests include design, fabrication, and characterization of III/V hybrid integrated nanophotonic silicon devices used in optical interconnects and RF sensing, including highly linear broadband graphene optical modulators, high-speed sub-volt low-dispersion E.A modulator based on Bragg reflector waveguide, and transverse-coupled-cavity VCSELs. He has published as the first author about 100 peer-reviewed papers in prestigious journals and conferences. Dr. Dalir holds 5 issued and 1 pending patents on ultra-high-speed devices. Dr. Dalir is a member of Optical Society of America (OSA) and fellow of JSPS.

Chi-Jui Chung received the B.S. degree in mechanical engineering from National Chiao Tung University, Hsinchu,

Taiwan, in 2009 and the M.S. degree in power mechanical engineering from National Tsing Hua University, Hsinchu, Taiwan, in 2011. From 2011 to 2014, he was with the Electronics and Opto-Electronics Research Laboratories, Industrial Technology Research Institute, Hsinchu, Taiwan. He is currently working toward the Ph.D. degree at the University of Texas at Austin, TX, USA. His current research interests include sub-volt photonic crystal waveguide modulators, broadband electromagnetic field sensors, and silicon based photonic true time delay system.

Xiaochuan Xu (M'15) received the B.S. and M.S. degrees in electrical engineering from the Harbin Institute of Technology, Harbin, China, in 2006 and 2009, respectively, and the Ph.D. degree in electrical and computer engineering from the University of Texas, Austin, TX, USA, in 2013. His current research interests include flexible photonics, nonlinear optics, fiber optics, and silicon photonics. Dr. Xu has published over 90 peer-reviewed journal and conference papers and holds three US patents. He is a member of IEEE, OSA and SPIE

Volker J. Sorger is an associate professor in the Department of Electrical and Computer Engineering, and the director of the Orthogonal Physics Enabled Nanophotonics (OPEN) lab at the George Washington University. He received his PhD from the University of California Berkeley. His research areas include opto-electronic devices, plasmonics and nanophotonics, including novel materials, and optical analogue information processing and neuromorphic computing. Amongst his breakthroughs are the first demonstration of a semiconductor plasmon laser, diffraction-limited waveguides, and sub 1-Volt plasmonic electro-optic modulator, optical FFT on-chip, and symmetry-detection via neuromorphic computing. Dr. Sorger received multiple awards among are the Early Career Award and Dean's Outstanding Young Research Award at GW, the AFOSR Young Investigator Award, Hegarty Innovation Prize, and the National Academy of Sciences award of the year. Dr. Sorger is the editor-in-chief of Nanophotonics, the executive chair overseeing all Technical Groups at OSA, and serves at the board-of-meetings at OSA and SPIE and the scholarship committee. He is a senior member of IEEE, OSA & SPIE.

Ray T. Chen (M'91–SM'98–F'04) Ray Chen is the Keys and Joan Curry/Cullen Trust Endowed Chair at The University of Texas Austin. He is the director of the Nanophotonics and Optical Interconnects Research Lab, at the Microelectronics Research Center. He is also the director of the AFOSR MURI center for Silicon Nanomembrane involving faculty from Stanford, UIUC, Rutgers, and UT Austin. He received his BS degree in Physics in 1980 from the National Tsing Hua University in Taiwan, his MS degree in physics in 1983, and his PhD degree in Electrical Engineering in 1988, both from the University of California. He joined UT Austin in 1992 to start the optical interconnect research program. From 1988 to 1992 Chen worked as a research scientist, manager, and director of the Department of Electro-Optic Engineering at the Physical Optics Corporation in Torrance, California. Chen served as the CTO, Founder, and Chairman of the Board of Radiant Research, Inc. from 2000 to 2001, where he raised 18 million dollars A-Round funding to commercialize polymer-based photonic devices involving over twenty patents, which were acquired by Finisar in 2002, a publicly traded company in the Silicon Valley (NASDAQ:FNSR). He also serves as the founder and Chairman of the Board of Omega Optics Inc. since its initiation in 2001. Omega Optics has received over five million dollars in research funding. His research work has been awarded over 135 research grants and contracts from such sponsors as Army, Navy, Air Force, DARPA, MDA, NSA, NSF, DOE, EPA, NIST, NIH, NASA, the State of Texas, and private industry. The research topics are focused on four main subjects: (1) Nano-photonic passive and active devices for bio- and EM-wave sensing and interconnect applications, (2) Thin film guided-wave optical interconnection and packaging for 2D and 3D laser beam routing and steering, (3) True time delay (TTD) wide band phased array antenna (PAA), and (4). 3D printed micro-electronics and photonics. Experiences garnered through these programs are pivotal elements for his research and further commercialization. Chen's group at UT Austin has reported its research findings in more than 860 published papers, including over 100 invited papers. He holds over 35 patents. He has chaired or been a program-committee member for more than 110 domestic and international conferences organized by IEEE, SPIE (The International Society of Optical Engineering), OSA, and PSC.

He has served as an editor, co-editor or coauthor for over twenty books. Chen has also served as a consultant for various federal agencies and private companies and delivered numerous invited talks to professional societies. Chen is a Fellow of IEEE, OSA, and SPIE. He was the recipient of the 1987 UC Regent's Dissertation Fellowship and the 1999 UT Engineering Foundation Faculty Award, for his contributions in research, teaching and services. He received the honorary citizenship award in 2003 from the Austin city council for his contribution in community service. He was also the recipient of the 2008 IEEE Teaching Award, and the 2010 IEEE HKN Loudest Professor Award. 2013 NASA Certified Technical Achievement Award for contribution on moon surveillance conformable phased array antenna. During his undergraduate years at the National Tsing Hua University he led the 1979 university debate team to the Championship of the Taiwan College-Cup Debate Contest. Chen has supervised and graduated 48 PhD students from his research group at UT Austin. Many of them are currently professors in the major research universities in USA and abroad.